

The separation techniques for secondary beams

Gottfried Münzenberg

Gesellschaft für Schwerionenforschung mbH, 6100 Darmstadt, Germany

In-flight separation of unretarded nuclear reaction products has made considerable progress in recent years. Electromagnetic separators for exotic species produced by nuclear fission, heavy ion fusion, target spallation, or projectile fragmentation have been developed to separate isotopes over the whole periodic table of elements with energies up to the GeV/u range.

Recently, the possibility to produce exotic nuclear beams with energies far above the Coulomb barrier by projectile fragmentation opened a new field of secondary beam physics, the direct use of isotopically separated beams of unstable nuclei for nuclear reactions. Characteristic examples of in-flight separation will be discussed with emphasis on the new generation of projectile fragment separators, including the future application of cooled and stored secondary beams for the application in nuclear physics.

1. Introduction

In this paper the separation of secondary beams produced in nuclear reactions will be discussed with the restriction to in-flight separation techniques, where the reaction products pass an electromagnetic separator unretarded with their full kinetic energy from the nuclear reaction process leading to their creation. Separators for recoils from heavy ion fusion and also for fission products have been reviewed in a number of papers, e.g. refs. [1–4]. This paper will include the most recent developments in the separation of relativistic nuclei created by projectile fragmentation, give a short overview on the production processes and the reaction kinematics, and discuss briefly the various separation techniques applied for exotic-beam production and their limitations.

2. Sources of exotic nuclear beams

The classic sources of energetic secondary beams to which in-flight separation is applicable are neutron induced fission, e.g. of heavy targets like uranium in high flux reactors, proton induced uranium spallation and complete fusion of heavy ions. Recently, developments have been made to use fragmentation of heavy projectiles to produce energetic beams of unstable nuclei with energies far above the Coulomb barrier, which can be used directly for secondary reactions.

The regions of the chart of nuclei accessed by these production methods are shown in fig. 1. The neutron induced uranium fission produces a light and a heavy group of nuclides around krypton and xenon, respec-

tively, and leads to neutron-rich isotopes because of the large excess of heavy elements. Proton induced fission creates symmetric fragments with a peak cross section near palladium. Heavy ion fusion, the amalgamation of two nuclei, generally leads to neutron-deficient heavy nuclei. This is the only type of reaction discussed here which creates products heavier than either of the initial nuclei. With this type of reaction the heaviest known elements have been produced. Projectile fragmentation, which is in principle spallation in inverse kinematics, leads to isotopes lighter than the projectile with peak cross sections close to the neutron-deficient side of the stable isotopes. All these reactions, except complete fusion, where only a few isotopes near the compound nucleus are formed, lead to broad isotopic distributions.

The kinematic properties of the reaction products such as average energy, energy spread, and angular distribution are determined by the mechanism of the nuclear reaction. Fission fragments gain their energy from the Coulomb repulsion of the fragments in the phase of their separation. The recoil energy of a fragment with mass A_f emerging from the mother nucleus with mass A can be obtained with the help of the Viola systematics for fission energies [5]:

$$E_r = 0.25 \frac{Z^2}{A^{4/3}} (A - A_f). \quad (1)$$

Heavy-ion fusion products suffer the full momentum transfer from the projectile. The recoil energy of a heavy evaporation residue is:

$$E_r = \frac{A_p}{A_c} E_p, \quad (2)$$

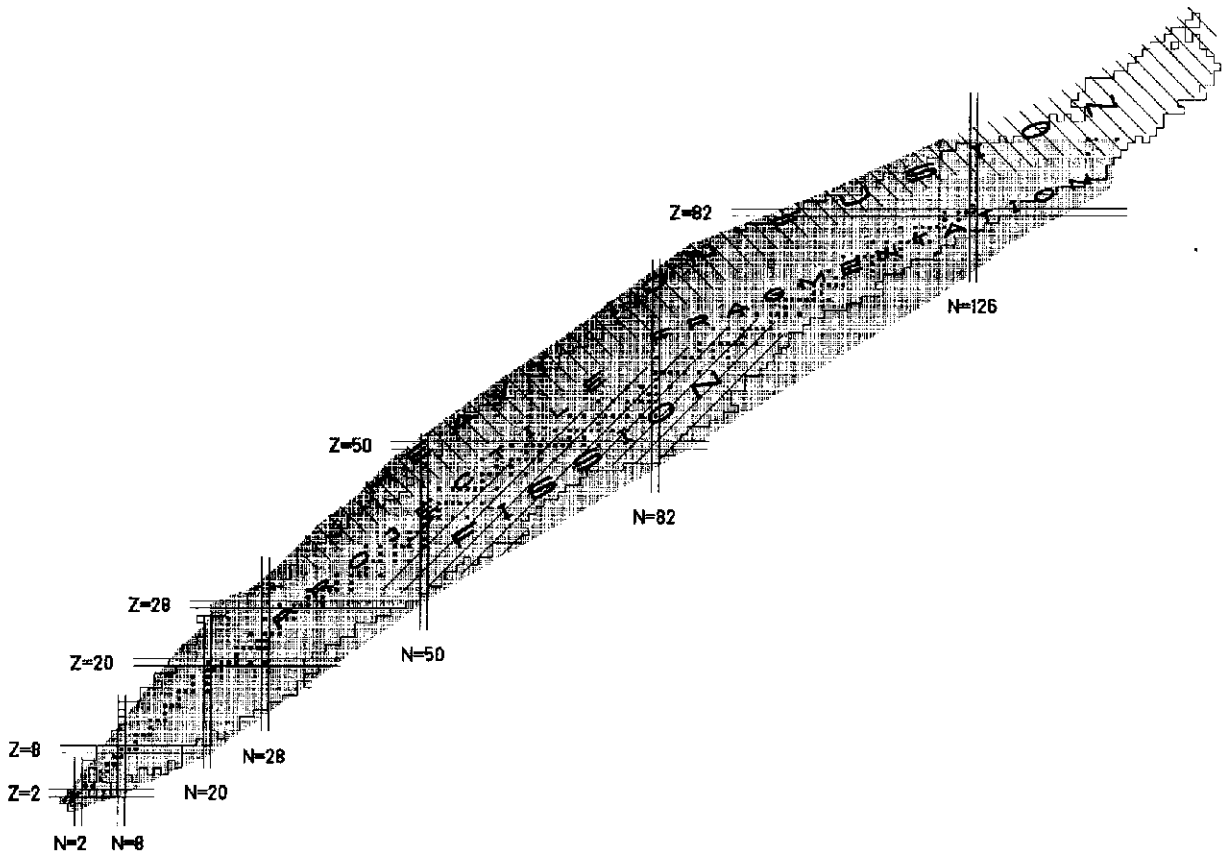


Fig. 1. Regions of the chart of nuclei which can be accessed by neutron induced fission, complete fusion of heavy ions, and fragmentation.

A_p and E_p denoting the projectile mass and energy, respectively, and A_c standing for the mass of the compound nucleus from which the evaporation residue emerges by particle evaporation. For the production of exotic species the projectile energy is chosen close to the Coulomb barrier, which for medium heavy and heavy nuclei is close to 5 MeV/u (fig. 2). The velocity

of projectile fragments is essentially the same as the velocity of the projectile, their energy being

$$E_{fr} = \frac{A_{fr}}{A_p} E_p. \quad (3)$$

These considerations show that all sources of secondary beams have energies below the Coulomb barrier and cannot be used for secondary reactions without further acceleration except for projectile fragments, which may have energies up to the GeV/u range (fig. 2). The energy of projectile fragments is only limited by the energy of the projectiles. Cyclotrons typically deliver beams up to 0.1 GeV/u; higher energies are available from synchrotrons. The figure also shows the energy limit where 50% of the ions are fully stripped. This is an important limit for efficient and clean ion optical separation.

The separation efficiency of in-flight separators depends on the phase-space populated by the production reaction. Separators accept typically less than 10 msr and less than about 5% in momentum spread.

Fission products are emitted into the full solid angle and with wide energy distributions (fig. 3); the separation efficiency is as small as 10^{-6} [3].

Evaporation residues from heavy ion fusion are kicked out of the target by the momentum transfer

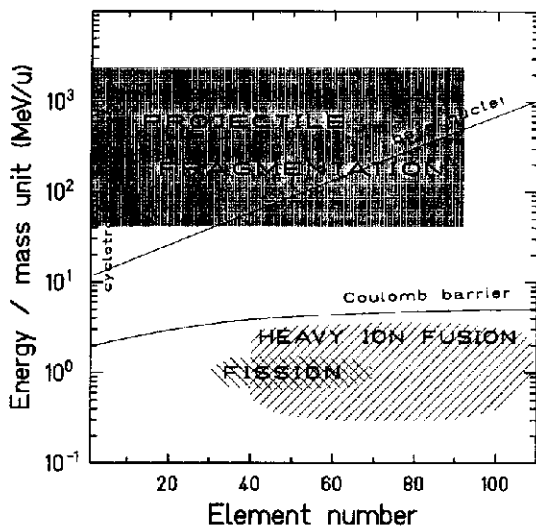


Fig. 2. Domains of kinetic energies of the reaction products from various nuclear reactions.

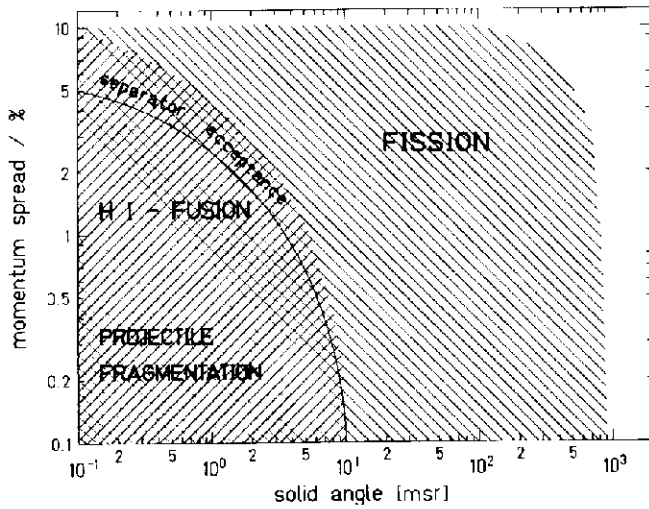


Fig. 3. Solid angle and momentum spread of the reaction products compared to the acceptances of spectrometers.

they suffer from the projectile; they are emitted into a narrow cone in the beam direction and with a small velocity spread. The phase-space population of the recoils is determined by the recoil momentum from the particles evaporated from the hot compound nucleus. If n particles are evaporated, the relative momentum spread of the recoils is [6]

$$\sigma_r/p_r = \sqrt{\sum_n p_i^2} / p_p, \quad (4)$$

where p_p and p_i are the momenta of the projectile and the i th evaporated particle, respectively. Typical values for fusion-evaporation products created with sufficiently heavy beams ($A > 40$) and with beam energies close to the Coulomb barrier are solid angles of less than 10 msr and velocity spreads of a few percent in the case of neutron evaporation, consequently the separation efficiencies are typically 10 to 100%.

Projectile fragments keep the velocity of the projectile; their momentum distribution is determined by the Fermi motion of the abraded nucleons and given by

Goldhaber [7]. The relative momentum spread in the beam direction is

$$\sigma_{tr}/p_{tr} \approx \frac{p_F}{\beta\gamma} \sqrt{\frac{n}{5A_p A_{fr}}}. \quad (5)$$

Here, p_F is the Fermi momentum, $p_F = 221$ MeV/c, and p_{fr} the momentum of the projectile fragment. For the transverse momentum spread σ_{tr} is slightly higher by 0.3 GeV/c. Eq. (5) shows that the momentum spread increases with the increase of the number of abraded nucleons, which means that the momentum spread of the fragments increases when they become more and more exotic. This effect becomes of increasing importance for light fragments. As the momentum spread of the fragments is independent of the projectile energy, they are well forward peaked at high energies. Typical values for solid angle and relative momentum spreads for heavy and relativistic fragments with $A > 100$ and $E/u = 500$ MeV/u are 1 msr and 2%. This fits well into the acceptance of high resolving spectrometers (Fig. 3). Separation efficiencies of 50 to 100% can be achieved.

2.1. Luminosities and production rates

The production rates for exotic species are determined by the beam currents available from the source of the primary beam (which may be a reactor to deliver neutrons for induced fission or an accelerator for energetic ion beams), the target thickness, and the nuclear reaction cross section.

The source strength can be characterized by the luminosity, which is defined as

$$L = \dot{N}_p N_t, \quad (6)$$

where \dot{N}_p and N_t are the beam current in particles per second and the number of target atoms per cm², respectively. The primary fluxes of neutrons in a high-flux reactor are 5×10^{14} /cm². Heavy ion and proton accelerators as linacs, cyclotrons or proton synchrotrons

Table 1
Secondary beam intensities for the various production methods

	Ind. fission	HI-fusion	Projectile fragmentation	
			$E/u < 100$ MeV/u	$E/u > 100$ MeV/u
Projectiles on target [s ⁻¹]	5×10^{14}	10^{13}	10^{13}	10^{10}
Target atoms [cm ⁻²]	10^{18}	10^{18}	10^{22}	10^{23}
Luminosity [s ⁻¹ cm ²]	5×10^{32}	10^{31}	10^{35}	10^{33}
Production cross section [cm ²]	$< 10^{-23}$	$< 10^{-25}$	2×10^{-25}	
Sec. rates [s ⁻¹]	$< 5 \times 10^9$	$< 10^6$	$< 10^{10}$	10^8
Separation efficiency	$10^{-4} - 10^{-6}$	0.2-1	0.1	1
Intensity of separated beam	$< 5 \times 10^5$	$< 10^6$	$< 10^9$	$< 10^8$

provide beams of 10^{13} /s; the beams presently available at heavy ion synchrotrons are smaller by about three to four orders of magnitude. Later generations with high current injectors will have comparative beam intensities.

Using recoil separators, target thickness is generally limited by the energy loss of the reaction products in the target, which is advantageous for relativistic projectile fragments; they are typically 1 mg/cm^2 for fission targets used in recoil separators and for fusion reactions [3]. They range typically from 0.1 to 1 g/cm^2 for projectile fragmentation. The corresponding luminosities are 10^{32} and $10^{31} \text{ cm}^{-2} \text{ s}^{-1}$ for fission and fusion, respectively, and range up to $10^{36} \text{ cm}^{-2} \text{ s}^{-1}$ for fragmentation (table 1).

The total nuclear reaction cross section is of the order of the geometric cross section, or even larger in the case of resonant neutron capture. The production cross section of a specific nuclear species in general, however, will be only a small fraction of this value, as many competing reaction channels are open. In the fission as well as in the fragmentation process a great number of isotopes are produced simultaneously just with one target-projectile combination. In the heavy ion fusion process only few nuclides are produced, which facilitates their separation.

The production cross section for a specific nuclear species ranges from the order of 10 to 1000 mb down to the picobarn region for the most exotic nuclei at the limits of stability.

Table 1 summarizes the secondary beam intensities for the three production methods discussed here. The rates for the most intense fission products obtained by in-flight separation are of the order of 5×10^5 for the most intense species; they may be as high as 10^7 for heavy ion fusion products. They range from 10^8 to 10^9 for projectile fragments, where the advantage of the high intensity of the cyclotron beams is partly compensated by the increase of target thickness and separator transmission, which can be used for the more energetic synchrotron beams.

3. Design principles and application of specific separation techniques

An overview of the ion optical principles of the various separation techniques for in-flight separation has been given recently [8]. Here, only some basic considerations for the applicability of the different techniques for the various kinds of reactions and energy regimes will be discussed (table 2).

Conventional ion optics uses magnetic and electric fields or a combination of both to achieve a resolution in momentum over charge, energy over charge or mass over charge, respectively. The theoretical limit of the

resolving power of such systems for particles of the magnetic rigidity BQ is governed by the emittance, $2x_0 \times 2x'_0$, of the beam to be separated, the usable field area S covered by this beam in the deflection field, and the bending radius ρ :

$$R_{BQ} = \frac{BS}{2x_0 2x'_0 BQ}, \quad (7)$$

where x_0 and x'_0 are the halfwidths of the beamspot and of the beam angle at the target, and B is the magnetic field strength.

A similar condition can be derived for the electrostatic separator. With E as the electric field strength and FQ as the electric beam rigidity, eq. (7) can be written for the electric field as

$$R_{F\rho} = \frac{ES}{2x_0 2x'_0 FQ} = \frac{VL}{2x_0 2x'_0 FQ}, \quad (8)$$

which gives the relation between the theoretical limit of the resolution and the total voltage V applied across the deflection condenser and the condenser length L . From eq. (8) it is evident that the application of electric fields to separate relativistic heavy ions is quite limited. A condenser of 20 m length with a voltage of 1 MV across the gap has an energy resolution of 50 for 0.5 GeV/u ions which decreases to 10 at 1 GeV/u [9].

The resolution of systems consisting of more than one deflection field is obtained by combination of these equations [10]. Such combinations can be used to cancel the velocity dispersion to obtain a mass over charge resolution, which is the classic Mattauch-Herzog design. In such combinations the mass-resolving power of the electric field is reduced by the relativistic factor $1/\gamma^2$. To eliminate the mass over charge dispersion to obtain a velocity separation, the classical Wien filter is used. In combination of electric and magnetic fields with the directions of deflection perpendicular to each other, the addition of the dispersion vectors cancels out the velocity dispersion for ions of a certain mass over charge ratio along a parabola, while the momentum and energy information are kept along the deflection directions of the magnetic and electric field, respectively. This is the Thomson design of the parabola spectrograph. Of course, it is unimportant from the ion optical point of view whether the fields are spatially separated or superimposed. All these possible field combinations have been used to separate fission products and fusion recoils [1-3].

Another possibility to achieve mass separation is the use of combinations of deflection magnets and RF-fields. Ions of certain velocity bands are separated. To obtain an optimal mass resolution the time-dependent dispersion of the RF-field is used. The resolution

of such separators at accelerators with a bunch length Δt is [11]

$$\frac{m}{\Delta m} = \frac{L}{c} \frac{\Delta t}{\beta \gamma^2}, \quad (9)$$

where L is the distance between RF-deflection and the target, and c is the velocity of light.

Due to the nature of the electromagnetic force all separators working on a purely ion optical basis separate ions according to their mass over charge ratio. In the low energy domain, where the ions are not fully stripped, a certain nuclear species is distributed over various ionic charge states, with abundances of 10 to 20% on the average [12]. To achieve a high separator transmission, gas filled separators can be used. In charge exchange collisions with the filling gas the ionic charge states of the trespassing ions fluctuate around the average charge state [3]:

$$\bar{q} \approx vZ^{1/3}. \quad (10)$$

The average deflection in magnetic devices now depends only on the nuclear charge and mass. Consequently, ions covering wide velocity and charge distributions are separated with high efficiency, however, due to straggling effects, energy loss, and the statistics of ionic charge exchange, with moderate resolution. The pressures to optimize the competing effects in those systems are of the order of torrs.

One advantage of recoil separators is that the ions leave the target ionized and no ion sources are needed. This is important especially in the region of refractory elements. The short separation time which is determined by the flight time through the separator counts in microseconds. Therefore, nuclei at the very limits of

stability, such as ground state proton emitters and the heaviest known elements, have been discovered and investigated with in-flight separators. Furthermore, the possibility to measure coincidences, for instance with processes occurring at the target, e.g. the de-excitation by fast gamma cascades, has been one great success of this kind of separator.

For relativistic ions new separation methods have been developed, as all separation methods discussed here have their drawbacks [9]. The most promising method used at present is the combination of magnetic separation and energy loss in a degrader [14–16]. The energy loss scales with:

$$\frac{dE}{dx} \propto Z^2/\beta^2, \quad (11)$$

and hence allows a discrimination according to the nuclear charge.

A separator of this type consists of an achromatic analyzer with a degrader placed at the intermediate dispersive focal plane. The whole system is tuned so that all fragments suffering the same differential loss in the degrader are focused at the exit of the separator. Such separators provide isotopically separated secondary beams. Evidently, the resolution of such a separator is limited by the energy straggling in the degrader. Fig. 4 shows that this method is limited to relativistic particles, as in this energy regime the relative broadening of the momentum spread, due to energy straggling of the particle to be separated, is sufficiently small. A drawback of this method for low energy ions is the fact that ionic charge exchange of not fully stripped ions leads to satellite peaks in the particle spectra.

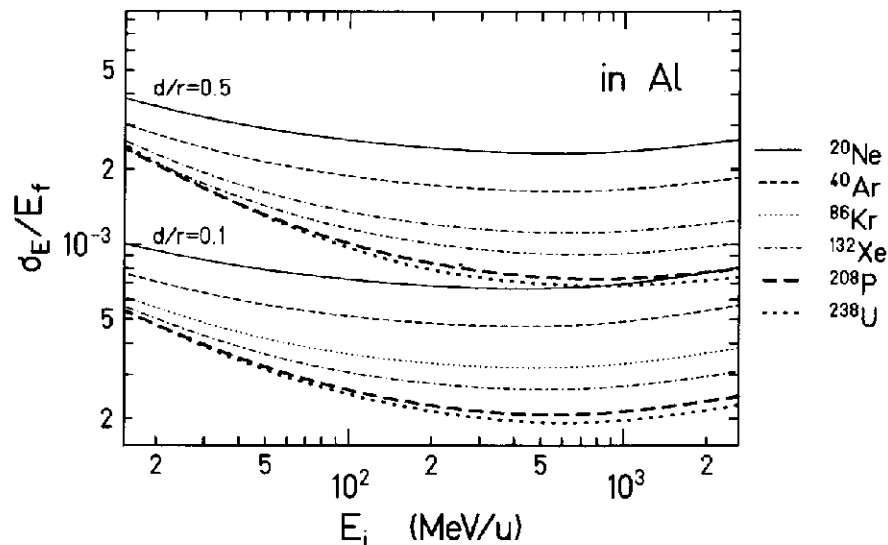


Fig. 4. Relative energy straggling of relativistic heavy ions in a degrader of 10% and half-range thickness, respectively, as a function of energy. The degrader material is aluminum [13].

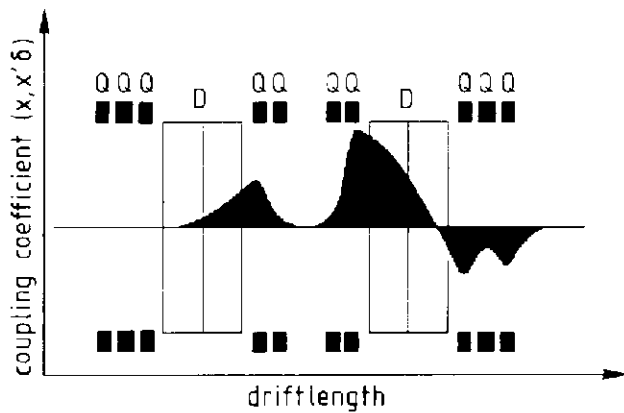


Fig. 5. Coupling coefficient for the chromatic aberration, calculated for two sections of the GSI fragment separator [13].

3.1. Corrections of aberrations

To obtain the theoretically possible resolutions it is necessary in most cases to correct for aberrations. For the ion optical correction elements to be effective, however, they must be placed in the correct position along the ion optical system. The coupling coefficients show how efficiently a correction element at a specific position corrects an aberration [17].

With the formalism of these coupling coefficients it can be achieved that a certain correction element influences only a specific aberration, which is of special importance if it is necessary to correct aberrations by tuning a separator on-line. As an example fig. 5 shows the strength of the coupling coefficient to the chromatic aberration for one section of the GSI fragment separator.

4. The different separator types and their applications

4.1. Recoil mass separators

The application of the various discussed separation methods for secondary beams is determined by the reaction kinematics, the energy spread and the isotopic resolution. In fact, all of the methods have been used successfully in the research with secondary beams. In the following section, an overview of a number of separators will be given and only specific new developments in this field will be discussed in detail. Table 2 shows a comparison of the various techniques and their main applications. Magnetic separators discriminate particles only according to their magnetic rigidity or momentum over charge ratio. As all sources of secondary beams deliver beams with considerably wide momentum spreads, an additional velocity determination is necessary to achieve a sufficient mass separation. Combinations of magnetic and electrostatic dipoles to achieve an energy-independent mass separation have already been used in early times for the separation of fission fragments [18]. Here the target is placed in the focus of the electric sector field, and the detector in the focus of the magnetic sector field to achieve a parallel beam between the deflection fields.

Modern recoil mass separators used for the separation of evaporation residues from heavy-ion fusion are collected in table 3. They employ quadrupole focusing. As a typical example, the Argonne Fragment Mass Analyzer (FMA) is shown in fig. 6. A quadrupole doublet at the separator entrance shapes the beam to illuminate the dispersive elements properly. The advantage of such a design is that the size of the deflection fields can be optimized with respect to resolution and transmission, as the illumination of the usable field

Table 2
The various ion optical methods of isotope separation

	Separation parameter	Limitations	Comments
<i>Low energy</i>			
Magn. spectrometer	p/q	$\Delta v/v$ determines $\Delta m/m$	for pre-separation
Recoil mass separator	A/q	E -field determines E_{\max}	ionic charge states create ambiguities
RF-separator	v	time structure determines $\Delta v/v$	
Gas filled magnet separator	A, Z	full stripping of ions	high transmission, weak resolution
<i>Intermediate energy</i>			
Magnetic achromat with energy degrader	A, Z	E -straggling in degrader determines $\Delta M/M, \Delta Z/Z$	kinematics enlarge beamspot

Table 3

Recoil mass separators. The abbreviations are Q: quadrupole, D: magnetic dipole, E: electric dipole, W: crossed-field Wien filter

	Configuration	Solid angle [msr]	$m/\Delta m$
Rochester [4]	QQQ EE QQQ	1-5	10^3-10^2
CARP [19]	QDEQ	3	320
LNC [20]	QQ EDE	5	280
FMA [21]	QQ EDE QQ	8	300
Daresbury [22]	QQQ WW QQQ	8	300
	D QQQ		
SHIP+NASE [23]	QQQ BDD	3	130
	DDE QQQ		
	DQQ		

area can be adjusted by the entrance quadrupoles. The use of an electric field as the first deflecting element is advantageous for the separation of heavy recoils from fusion. The projectile beam is separated efficiently due to the reaction kinematics (eq. (2)). The splitting of the electric fields has the effect that the projectile beam will not hit the condenser plates. Separators of this type are compact and have a high transmission because of the strong focusing of the quadrupoles. Other recoil mass analyzers use a combination of a velocity filter and a dispersion-matched magnetic dipole. As velocity filters are charge refocusing, they eliminate background from projectiles with exotic charge states. Fig. 7 shows the Daresbury separator. The employment of two velocity filters allows efficient separation of the projectile background. The class of RF-separators will not be described here as their application is rather special; gas filled separators cannot deliver isotopic beams because of their poor resolution of $A/\Delta A = 79$ and $Z/\Delta Z = 38$ [3].

Table 4

Separators for projectile fragments, courtesy of A. Artukh [26]

	LISE France 1984	SPEG France 1985	SPEG + d France 1986	RIKEN Japan 1989	GSI FRG 1990	NSCL USA 1991	LNR Dubna 1992
Configuration	2QD2Q Fd2QD 2QFa(2Q)	2QS2D QFd	α -channel + SPEG	3QSDSQ Fd2QSD S3QFa 3QFa2QFa	3QD2QFd 2QD3QFd 3QD2QFd 2QD3QFa	3QSD2Q Fd3QFd2 QSDSD 3QFa	2D2Cd Fd2Cd 2DFa(2Q)
$\Delta\Omega$ [msr]	1.0	4.9	1.0	5.0	0.7-2.5	0.3-4.3	6.4
$\Delta p/p$ [%]	± 2.5	± 2.5	± 0.5	± 3.0	± 1.0	± 1.5	± 10
$Rp/\Delta p$	800	10000	2000	2000	8000	3400	4360 (8720)
$B\rho$ [Tm]	3.2	2.8	2.8	5.76	5-18	5.4-7.2	4.5
Tag. [g/cm ²]	~ 0.2	~ 0.2	~ 0.2	~ 1.0	0.1-10	~ 1.5	< 1.0
Length [m]	18(24)	13.8	82	21(27)	74	19(22)	14.5(18)
Mode	achrom.	disp.	disp.	achrom.	achrom.	achrom.	achrom.

TARGET

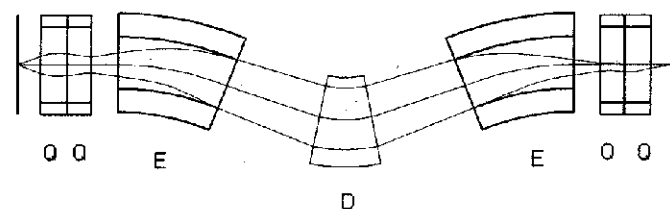


Fig. 6. The Argonne fragment mass analyzer.

4.2. Fragment separators

For heavy ions of intermediate energy a new type of separator is used: The combination of magnetic analysis and energy loss in solid material. This has two reasons: the application of high voltage deflectors of technical feasibility and considerable resolution is limited to about 100 MeV/u (eq. (8)), and, secondly, the energy-loss straggling of relativistic ions becomes so small (fig. 4) that the energy loss of particles can be determined with sufficient precision to measure the nuclear charge reliably even for the heaviest ions, an observation well known from the application of ionization chambers. A description of recently built or planned facilities is given in the proceedings of the conferences on radioactive beams held to date and in the proceedings of this conference [24,25]. An overview of existing and planned fragment separators is given in table 4.

The LISE separator at GANIL [14,15] which was first used to separate exotic beams from projectile fragmentation in a large scale experimental program is shown in fig. 8. LISE is a large magnetic forward spectrometer of high resolution. It consists of two identical magnetic dipoles with a deflection angle of 45°, a configuration of QQDQQ QQDQQ QQ, and is symmetric with respect to the central dispersive focal

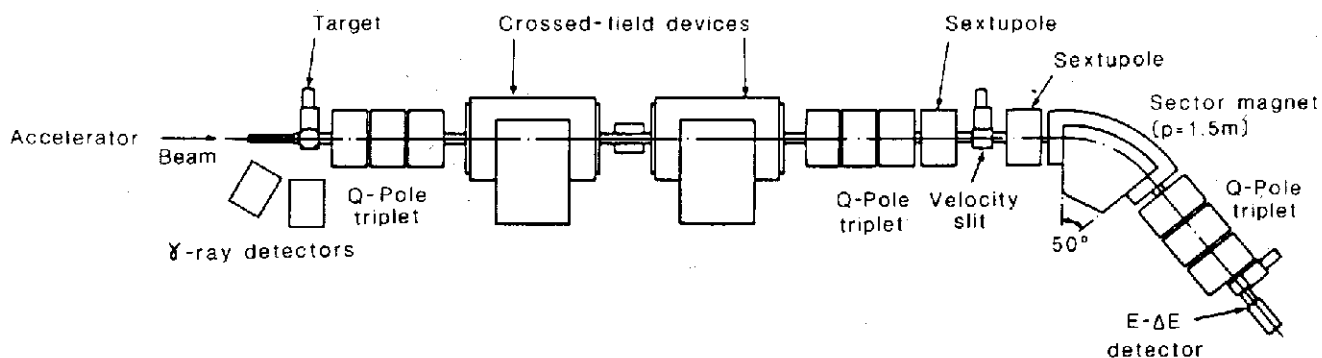


fig. 7. The Daresbury recoil mass separator.

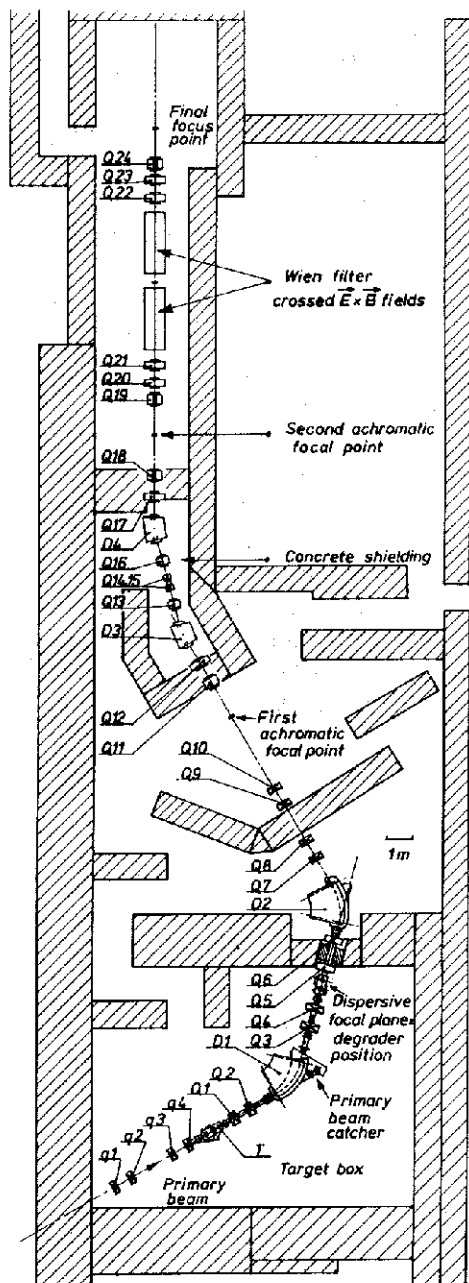


Fig. 8. The LISE separator in its latest version: combined with a velocity filter, courtesy of D. Guillemaud Mueller.

plane but extended by a quadrupole doublet at the exit. The separation principle is explained in fig. 9. The first stage of the separator selects in A/Z , as all ions passing the separator are fully stripped. It selects a band of isotopes along the line $A/Z = \text{const.}$, the width of which is determined by the velocity spread of the fragments. The energy loss in the degrader is analyzed in the second part of the separator in terms of momentum change, which puts a second cut in the A, Z plane. As a result, a single isotope can be selected. For low energies and light isotopes the momentum distribution of projectile fragments is comparatively broad (eq. (5)), which spoils the isotopic selection. Therefore, LISE has been extended recently by a crossed-field velocity selector to include velocity analysis (fig. 9). This filter has the configuration QQ WW QQQ, and the Wien filter is divided into two subsections each of which has a length of 2.5 m. The condensers can be operated with a voltage of 300 kV across a 10 cm gap [27].

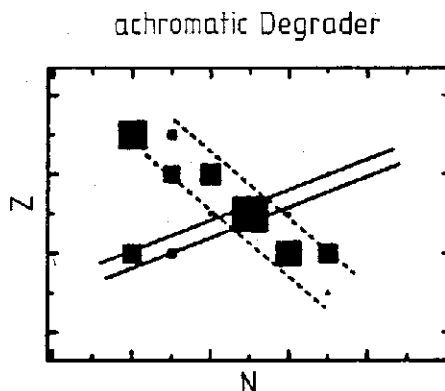


Fig. 9. The isotopical separation of projectile fragments. The magnetic separation of the fragments cuts along constant A/Z (solid lines). The second cut is made by the energy loss in the degrader (dashed lines).

4.3. The energy degrader – non-Liouvillean optics

The trespassing ions dissipate energy in the degrader, therefore Liouvillean optics is no longer applicable. Nevertheless, it is possible to find a beam transfer matrix for the degrader, including the A and Z dependences of the beam parameters [28]; consequently, the energy degrader can be used like a conventional ion optical element. The non-Liouvillean optics of the degrader has been discussed in ref. [29]. As all ion optical quantities scale in relative units, the energy loss in the degrader creates a mismatch in the dispersions between the two separator stages. If the dispersion of the first separator stage is D , the dispersion of a beam with the central momentum p_0 is

$$x(p) = D \Delta p / p_0. \quad (12)$$

The new momentum p_1 behind the degrader is substantially smaller, whereas the momentum spread Δp does not change to first order. Consequently, the dispersion must be compressed to match the dispersions, if the symmetry of the separator is to be maintained. This can be achieved by shaping the degrader accordingly with a wedge of appropriate angle [14]. A change of the magnification of one separator stage would, of course, have the same effect; however, symmetry would be lost. Evidently, an increase of the wedge angle would further bunch the momentum distribution of the

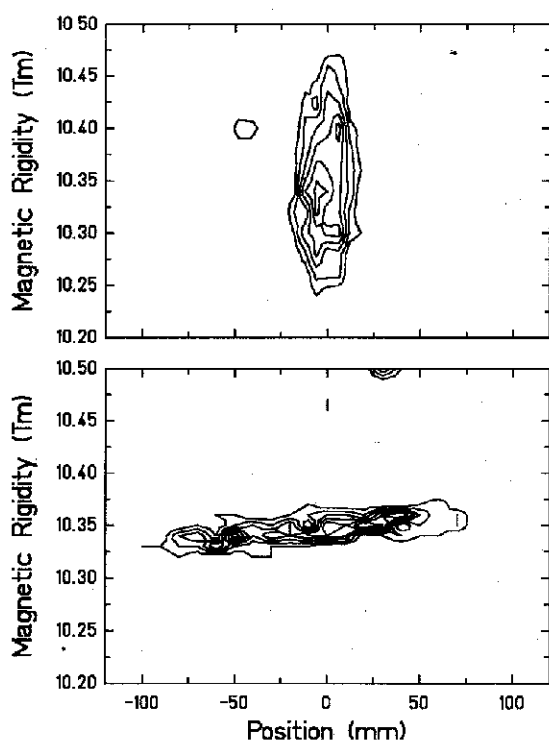


Fig. 10. Contour plots of the particle distributions at the final focus of the GSI fragment separator for the achromatic (upper panel) and the monoenergetic setting (lower panel) of the degrader. The coordinates are position and magnetic beam rigidity [30].

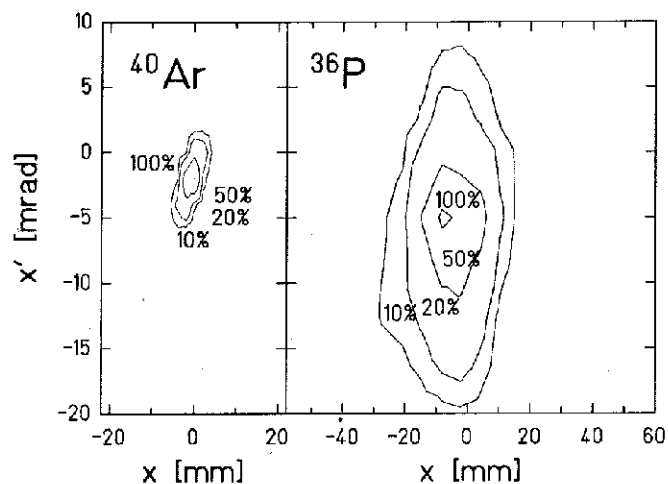


Fig. 11. Comparison of the emittances of the projectile beam (left panel) and the beam of separated projectile fragments (right panel) from the example of ^{36}P produced by fragmentation of 1 GeV/u ^{40}Ar [31].

beam, until an optimum value whereby the momentum spread of the particles is only determined by the separator resolution and the energy straggling in the degrader (fig. 10). This demonstrates the interplay between momentum spread and beam emittance. As a part of the momentum space is shuffled into the x, x' space, beam emittances of the fragment beams are comparatively large. The beam width x_1 at the final focus is due to this effect [29]:

$$x_1 = V_1 \left(V_2 + \gamma^2 D_2 \frac{dv}{dx_1} \right) x_0, \quad (13)$$

where V_1 and V_2 are the magnifications of the first and second separator stages, respectively, and dv/dx_1 is the velocity gradient created by the angle of the degrader wedge. This effect is illustrated in fig. 11, where the emittance of the initial projectile beam from the GSI heavy ion synchrotron SIS is compared to the emittance of a fragment beam. This example shows ^{36}P produced by fragmentation of ^{40}Ar of 1 GeV/u from an experiment at the GSI projectile fragment separator. While the emittance of the projectile beam is as small as 1.8π mmmrad, the fragment beam has an emittance of 44π mmmrad.

5. Secondary beams for nuclear reactions

The separators discussed in the previous sections have been used up to now predominantly for studies of exotic nuclei in the ground state or in their various modes of excitation and shapes not far from it. The creation of exotic nuclear beams with energies far above the Coulomb barrier, however, allows the study of nuclear reactions. This new generation of exotic-

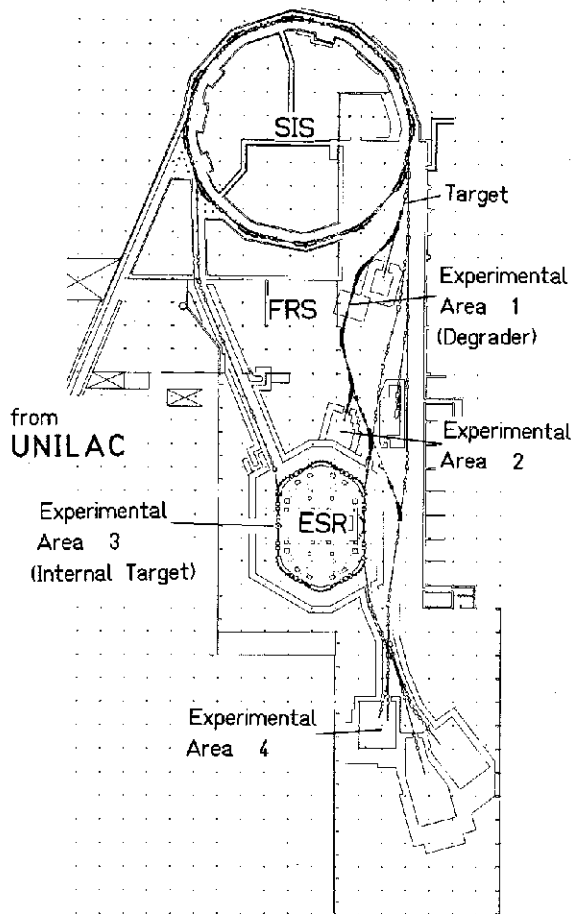


Fig. 12. The GSI heavy ion synchrotron SIS and the projectile fragment separator FRS with a dedicated experimental area (experimental area 2) and the beam line to the experimental storage and cooler ring ESR. ESR is equipped with the electron cooler and the internal gas target (experimental area 3). After passing ESR, radioactive beams can be transported to the experimental area for relativistic-beam experiments (experimental area 4).

beam experiments has been pioneered in Berkeley. In these experiments, interaction cross sections of light exotic projectile fragments with energies from several hundred MeV/u to some GeV/u were measured on an event-by-event basis using particle telescopes and the HISS magnet [16]. A disadvantage of such experiments is the small phase-space density of the fragment beams. To define the phase space of the fragments event by event, their coordinates have to be determined by particle tracking, which is limited by the detector resolution and the maximum countrate of the setup.

High phase-space density can be achieved by beam cooling. This new technique will be applied at GSI, where the projectile fragment separator FRS has a connection to the storage and cooler ring ESR (fig. 12). Fragment beams can be cooled and decelerated to cover the energy range from 500 to 3.5 MeV/u. Exper-

iments in the ring with an internal target are possible, as well as experiments with extracted beams which can be led to practically all experimental areas [30,31].

The FRS has four sections, each of the configuration QDQDQ. The separator at present has two exits: One leading to a dedicated experimental area, the other leading to the entrance of the storage ring. First results for electron cooling of relativistic, heavy ion beams have been obtained for ^{40}Ar , ^{86}Kr , and ^{209}Bi beams. The momentum spread of the cooled beams at energies close to 150 MeV/u was as small as 5×10^{-6} , and the beam emittance was 0.05π mm mrad [32].

6. Summary

The development of separation techniques for secondary beams has made considerable progress in recent years. Interesting and important contributions to the physics of exotic nuclei, such as the detection of short-lived species at the limits of nuclear stability (ground state proton emitters or the heaviest elements) or the investigation of nuclear matter in exotic states, as superdeformation was only possible using in-flight separation techniques. A new generation of experiments to investigate nuclear reactions with secondary beams has already been started with the measurement of reaction cross sections of neutron-rich light nuclei. For the future, the use of cooled secondary beams over large energy ranges will open a wealth of experimental possibilities with secondary beams of high brilliance and well defined energy.

Acknowledgements

The author gratefully acknowledges helpful discussions with H. Geissel, Y. Fujita, A. Magel, K.H. Schmidt and K. Sümmerer.

References

- [1] H.A. Enge, Nucl. Instr. and Meth. 186 (1981) 413.
- [2] H.A. Enge, in: Treatise on Heavy Ion Physics, vol. 7, ed. A. Bromley (Plenum, New York, 1985) p. 403.
- [3] P. Armbruster, 3rd Int. Conf. on Nuclei far from Stability, Cargese, Corsica, 1976, CERN Rep. 76-13.
- [4] T.M. Cormier, Ann. Rev. Part. Sci. 37 (1987) 537.
- [5] V.E. Viola Jr., K. Kwiatkowski and M. Walker, Phys. Rev. C31 (1985) 1550.
- [6] G. Münzenberg, W. Faust, S. Hofmann, P. Armbruster, K. Güttner and H. Ewald, Nucl. Instr. and Meth. 161 (1979) 65.
- [7] S. Goldhaber, Phys. Lett. 53B (1974) 306.
- [8] H. Wollnik, Nucl. Instr. and Meth. B26 (1987) 267.

- [9] H. Geissel et al., Projectile fragment separator, a proposal for the SIS-ESR experimental programme, Gesellschaft für Schwerionenforschung (GSI), Darmstadt, Germany, 1987, unpublished.
- [10] H. Wollnik, G. Münzenberg and H. Ewald, Nucl. Instr. and Meth. 111 (1973) 355.
- [11] G. Hinderer, Internal Report Gesellschaft für Schwerionenforschung (GSI), Darmstadt, Germany (1984) p. 97.
- [12] T.S. Nikolaev and T.S. Dmitriev, Sov. Phys. Tech. Phys. 15 (1971) 1383.
- [13] Th. Schwab, Thesis University Giessen, GSI Report, Darmstadt (1990).
- [14] J.P. Dufour et al., Nucl. Instr. and Meth. A248 (1986) 267.
- [15] R. Anne, D. Bazin, A.C. Mueller, J.C. Jacmart and M. Langevin, Nucl. Instr. and Meth. A257 (1987) 215.
- [16] I. Tanihata, in: Treatise on Heavy Ion Science, vol. 8, ed. A. Bromley (Plenum, New York, 1989) p. 443.
- [17] K.L. Brown, Internal Report Stanford, CA, SLAC PUB 3381 (1984).
- [18] H. Ewald, E. Konecny, H. Opower and H. Rösler, Z. Naturforsch. 19a (1964) 194.
- [19] S. Morinobu et al., Annual Report RNCP, Osaka, Japan (1980) p. 208.
- [20] P. Spolaore et al., Nucl. Instr. and Meth. A238 (1989) 381.
- [21] C.N. Davids, Proc. 1st Int. Conf. on Radioactive Nuclear Beams, Berkeley, CA, USA (World Scientific, Singapore, 1989) p. 174.
- [22] A.N. James et al., Nucl. Instr. and Meth. A267 (1988) 144.
- [23] G. Münzenberg et al., Nucl. Instr. and Meth. B26 (1987) 294.
- [24] J.M. Nitschke (ed.), Proc. 1st Int. Conf. on Radioactive Beams, Berkeley, CA, USA (World Scientific, Singapore, 1989).
- [25] Th. Delbar (ed.), Proc. 2nd Int. Conf. on Radioactive Beams, Louvain la Neuve, Belgium, 1991 (Adam Hilger, Bristol, 1992).
- [26] A.G. Artukh et al., Nucl. Instr. and Meth. A306 (1991) 123.
- [27] A.C. Mueller and R. Anne, Proc. 1st Int. Conf. on Radioactive Nuclear Beams, ed. J.M. Nitschke (World Scientific, Singapore, 1989) p. 132.
- [28] K.H. Schmidt, E. Hanelt, H. Geissel, G. Münzenberg and J.-P. Dufour, Nucl. Instr. and Meth. A260 (1987) 287.
- [29] H. Geissel et al., Nucl. Instr. and Meth. A282 (1989) 247.
- [30] J. Weckenmann et al., GSI Annual Report 1990, Darmstadt, GSI 91-1 (1991) 286.
- [31] M. Steiner et al., GSI Annual Report 1990, GSI 91-1 (1991) 285.
- [32] F. Bosch, Proc. 5th Int. Symp. on Radiation Physics, Dubrovnik, Croatia, Yugoslavia, 1991, Nucl. Instr. and Meth. A314 (1992) 269.